Published in final edited form as:
Cell. 2009 July 10; 138(1): 160–171. doi:10.1016/j.cell.2009.04.047.

A systems-level analysis of perfect adaptation in yeast osmoregulation

Dale Muzzey[1,2,4], **Carlos A. Gómez-Uribe**[1,3,4], **Jerome T. Mettetal**[1], and **Alexander van Oudenaarden**[1,*]

[1] Department of Physics, Massachusetts Institute of Technology, Cambridge, MA 02139, USA

[2] Harvard University Graduate Biophysics Program, Harvard Medical School, Boston, MA 02115, USA

[3] Harvard-MIT Division of Health Sciences and Technology, Massachusetts Institute of Technology, Cambridge, MA 02139, USA

SUMMARY

Negative feedback can serve many different cellular functions, including noise reduction in transcriptional networks and the creation of circadian oscillations. However, only one special type of negative feedback ("integral feedback") ensures perfect adaptation, where steady-state output is independent of steady-state input. Here we quantitatively measure single-cell dynamics in the *Saccharomyces cerevisiae* hyperosmotic shock network, which regulates membrane turgor pressure. Importantly, we find that the nuclear enrichment of the MAP kinase Hog1 perfectly adapts to changes in external osmolarity, a feature robust to signaling fidelity and operating with very low noise. By monitoring multiple system quantities (e.g., cell volume, Hog1, glycerol) and using varied input waveforms (e.g., steps and ramps), we assess the network location of the mechanism responsible for perfect adaptation in a minimally invasive manner. We conclude that the system contains only one effective integrating mechanism, which requires Hog1 kinase activity and regulates glycerol synthesis but not leakage.

INTRODUCTION

Positive and negative feedback loops are ubiquitous regulatory features of biological systems in which the system output reinforces or opposes the system input, respectively. Quantitative models are increasingly being used to study the function and dynamic properties of complicated, feedback-laden biological systems. These models can be broadly classified by the extent to which they represent specific molecular details of the network. At one extreme are the exhaustive models that dynamically track quantities of virtually all biomolecules in a system, often using differential equations based either on known or assumed reaction stoichiometries and rates. At the other end of the modeling spectrum is the minimalist approach, which aims to fit and predict a system's input-output dynamics with only a few key parameters, each potentially the distillation of a large group of reactions.

[*]Corresponding author: avano@mit.edu; 617-253-4446.
[4]These authors contributed equally to this work

Examples of exhaustive and minimalist modeling approaches illustrate their unique advantages and disadvantages. For instance, an exhaustive model of EGF-receptor regulation (Schoeberl et al., 2002) can impressively predict the dynamics of 94 specific network elements, but it requires nearly 100 parameters—some of which are not easily measured biochemically—and could suffer from the omission of important reactions not yet biologically identified. By contrast, minimalist models frequently lack such potentially desirable reaction- and network-specific details, yet they excel at providing intuitive and general insights into the dynamic properties of recurrent system architectures. For instance, two elegant studies of bacterial chemotaxis—a system said to "perfectly adapt" because abrupt changes in the amount of ligand only transiently affect the tumbling frequency, whereas steady-state tumbling is notably independent of the ligand concentration—highlighted a general feature of all perfectly adapting systems (Barkai and Leibler, 1997; Yi et al., 2000). Specifically, it was shown that a negative feedback loop implementing "integral feedback" is both necessary and sufficient for robust perfect adaptation in any biological system (Yi et al., 2000). Mathematically, a dynamic variable (e.g., x or $[cyclin\text{-}B]$) is an "integrator" if its rate of change is independent of the variable itself (e.g., if the dx/dt and $d[cyclin\text{-}B]/dt$ equations contain no terms involving x or $[cyclin\text{-}B]$, respectively), and integral feedback describes a negative-feedback loop that contains at least one integrator. Biologically, a biomolecule acts as an integrator if its rate equation is not a function of the biomolecule concentration itself; such a situation arises if, say, the synthesis and degradation reactions are saturated (Supplemental Data). By providing specific mechanistic constraints that apply to any perfectly adapting system, these two studies underscored the function and significance of perfect adaptation in homeostatic regulation and demonstrated the power of the minimalist modeling approach.

Both exhaustive and minimalist modeling tactics have been successfully applied to the osmosensing network in the budding yeast *Saccharomyces cerevisiae* (Klipp et al., 2005; Mettetal et al., 2008). The core of this network is a highly conserved mitogen-activated protein kinase (MAPK) cascade, one of several such cascades in yeast that regulate processes ranging from mating to invasive growth while being remarkably robust to cross-talk despite their many shared components (Hohmann, 2002; Schwartz and Madhani, 2004). Yeast cells maintain an intracellular osmolarity in excess of the extracellular osmolarity, thereby creating positive turgor pressure across the cell wall and membrane that is required for many processes including budding itself. Sudden drops in turgor pressure, potentially caused by an upward spike in the external osmolyte concentration, are detected by membrane proteins such as Sln1 (Reiser et al., 2003), which rapidly initiates a MAPK cascade culminating in the dual phosphorylation of the MAPK Hog1 (Figure 1A). Upon dual phosphorylation, the normally cytoplasmic and inactive Hog1 becomes activated and translocates to the nucleus (Ferrigno et al., 1998), where it plays direct and indirect roles in a broad transcriptional response (O'Rourke and Herskowitz, 2004). Glycerol-producing factors are among the activated genes, and they facilitate osmoadaptation through the increase of intracellular osmolarity (Hohmann et al., 2007). In fact, glycerol accumulation has been shown to comprise 95% of the internal osmolarity recovery (Reed et al., 1987). The subsequent restoration of turgor pressure leads to nuclear export of Hog1, which is dephosphorylated by several nuclear and cytoplasmic phosphatases.

Non-transcriptional mechanisms also play an important role in the hyperosmotic-shock response. Some are independent of Hog1 (e.g., rapid closure of Fps1 channels, which otherwise allow passive leakage of glycerol (Luyten et al., 1995; Tamás et al., 2000)), but others involve feedback mediated by the Hog1 pathway (Dihazi et al., 2004; Proft and Struhl, 2004; Westfall et al., 2008). For instance, in response to hyperosmotic stress, the glycolytic protein Pfk26, which stimulates production of glycerol precursors, was found to be activated via phosphorylation at MAPK consensus sites in a Hog1-dependent manner

(Dihazi et al., 2004). Additionally, in a recent study by Thorner and colleagues, it was shown that Hog1 sequestered in the cytoplasm can still mount an effective osmotic response (Westfall et al., 2008).

Biochemical characterization of most systems is rarely so rich to be deemed exhaustive, nor so minimal to consider a system as a black box. Thus, models combining elements from both approaches can be quite useful, such as a recent study that started with the exhaustive osmoadaptation model (Klipp et al., 2005) and abstracted several elements to yield a reduced representation (Gennemark et al., 2006). Here we take the reverse strategy, starting instead with the minimalist model (Figure 1B) and then using biological measurements and engineering principles to better understand systems-level dynamics and their relation with network topology.

In this study, we monitor the single-cell dynamics at high temporal resolution of both cell volume and Hog1 nuclear enrichment simultaneously in response to hyperosmotic stress. We observe perfect adaptation of Hog1 nuclear enrichment in response to step inputs of osmolyte; this adaptation occurs with very low cell-to-cell variability and is robust to the signaling fidelity of the MAPK cascade. From extensive theory developed in control engineering, we know that perfect adaptation in this feedback system requires an integral-feedback mechanism. We refine the position(s) of integrator(s) in our network by generating a range of putative network configurations and systematically rejecting those inconsistent with our data. Facilitating this process of elimination is our observation that perfect adaptation requires Hog1 kinase activity but not new protein production, suggesting that Hog1 may implement integral-feedback via a yet-unknown role in protein-protein interactions that increase the internal osmolyte concentration. Measurements of glycerol accumulation suggest that this crucial role for Hog1 kinase activity upregulates glycerol synthesis but does not otherwise regulate its leakage. Finally, in an experiment imposing severe constraints on the possible valid network configuration, we show that neither cell volume nor Hog1 nuclear enrichment perfectly adapts in response to a ramp input of salt. Together, our results establish that the system's negative feedback loop contains exactly one effective integrating mechanism. Though the loop may branch such that this effective integrator is composed of multiple integrating reactions arranged in parallel, we can reject the possibility that the net feedback loop contains two or more effective integrating mechanisms arranged in series.

RESULTS

MAPK Cascade Introduces Negligible Noise While Transducing Osmotic-Shock Signal

To gain further insight into Hog1 signaling dynamics and the feedback mechanisms that underlie osmoadaptation, we assayed the nuclear accumulation of Hog1 and cellular volume in single cells over time in response to hyperosmotic shock. We fused a yellow-fluorescent protein (YFP) to the C-terminus of endogenous Hog1 (Hog1-YFP) in haploid cells from which *SHO1* was deleted. *SHO1* deletion disables one of the two primary branches that activate Hog1, leaving the Sln1 branch as the main activator of Hog1. Importantly, *SHO1* deletion eliminates crosstalk with other MAPK cascades (McClean et al., 2007; Schwartz and Madhani, 2004) while still preserving the Hog1 dynamics (compare Figure 2A and Figure S1, (Hersen et al., 2008)) and gene expression profiles (O'Rourke and Herskowitz, 2004) of cells where both branches are intact. To identify the nucleus and thereby facilitate our computation of nuclear Hog1 enrichment, we also fused a red fluorescent protein to Nrd1 (Nrd1-RFP), a strictly nuclear factor. Throughout this work, we refer to this strain as "wildtype".

We created a simple flow-chamber apparatus to permit the changing of media with simultaneous acquisition of images. Cells were grown to log phase and loaded into the chamber (Figure 1C), where they adhered to a coverslip coated with concanavalin A. Media with or without excess osmolyte was washed over the cells throughout each experiment, and in less than two seconds the media within the chamber could be switched completely between the two types (data not shown). At each time point, we acquired phase-contrast, YFP, and RFP images, allowing us to observe a transient enrichment of Hog1 accumulation in the nucleus shortly after a hyperosmotic shock and diminished localization shortly before and long after the shock (Figure 1D).

We developed custom image-analysis algorithms to quantify the dynamic decrease in single-cell volume and increase in Hog1 nuclear enrichment in response to a step increase (Figure 2A) of the extracellular osmolyte concentration. For each cell, we compute the ratio of nuclear YFP signal to whole-cell YFP signal throughout the experiment, and define a cell's Hog1 nuclear enrichment as the relative change from the pre-shock level of this ratio (Experimental Procedures). Single-cell volume dynamics were computed from measurements of cell area (Experimental Procedures) and were interpreted as a proxy for turgor pressure. Single-cell Hog1 and volume data from a representative flow-cell experiment are posted on the *Cell* website. We observed remarkably low cell-to-cell variability in the network response, which includes the reactions in the MAPK cascade: for different cells, the amplitude and timing of changes in Hog1 nuclear enrichment and cell volume are very similar, with trends that closely follow the population average (Figure 2A, B). In fact, fluctuations in unstimulated cells were of a similar magnitude (Figure S2), further indicating that the intrinsic noise of signal propagation is low and suggesting that the experimental setup itself may be the predominant source of noise in our data. Compared with the recent observation of significant cell-to-cell variability in the dynamic nuclear enrichment of the yeast calcium-stress regulator Crz1 (Cai et al., 2008), these data suggest that the osmoadaptation signaling system generates output signals with very low noise, despite the fact that the system itself contains many proteins expressed at noisy levels (Newman et al., 2006).

Since our flow-cell-based assay allows for simultaneous measurement of cell volume and Hog1 nuclear localization at unprecedented timescales, we sampled the osmotic response every two seconds in response to a step of salt (Figure 2C, D). Again, we argue that the MAPK cascade generates negligible noise since the cell-to-cell variability in both the input (volume) and output (nuclear Hog1) are comparable. Together with the data from Figure 2A, B, this data gathered every two seconds reveals four distinct regimes in the relationship between cell volume and Hog1 activation in response to osmotic stress (Figure 2E). Within the first 20 seconds following a step of salt, cell volume drops precipitously, but Hog1 nuclear enrichment remains at its basal level while the stress signal propagates through the MAPK cascade. Between 20 seconds and 90 seconds, Hog1 nuclear enrichment rises from its minimum to its maximum but does not yet affect turgor pressure, as cell volume remains at its minimum. Shortly thereafter, turgor pressure begins to restore, and Hog1 nuclear enrichment begins to fall, with both reaching their pre-shock levels simultaneously at 25 minutes post-shock. Finally, cell growth resumes, as the cell volume grows and Hog1 returns to its basal level.

Hog1 Nuclear Enrichment Perfectly Adapts

We found that the steady-state Hog1 nuclear enrichment is identical to its pre-stimulus level over a range of hyperosmotic-shock strengths (Figure 3A). This dynamic behavior is the hallmark of perfect adaptation. Importantly, Hog1 perfect adaptation is not NaCl-specific, as we observed it with KCl and sorbitol treatment as well (Figure S3). In our simultaneous measurements of cell volume and Hog1 localization, we found a very strong correspondence

between the timing of both Hog1 adaptation and the restoration of turgor pressure, which we interpret as the moment that the rate of volume growth (i.e., slope of volume curve) in stressed cells matches that of unstressed cells (Figure 3A, B). Interestingly, for cells stressed with media containing 0.6M NaCl, this turgor pressure recovery appears to occur at a volume less than the pre-shock cell volume. This observation is consistent with membrane invagination that has been shown previously to occur only in cells under acute hyperosmotic stress (Slaninová et al., 2000): by decreasing membrane surface area, a particular turgor pressure can be achieved at a smaller volume.

We conclude from these data that the Hog1 nuclear enrichment level perfectly adapts and that this behavior is tightly coupled with perfect adaptation of turgor pressure. Taken together with extensive theoretical analysis of adaptive systems in engineering disciplines, these findings require that the system implement integral-feedback control (Ingalls et al., 2006; Sontag, 2003; Yi et al., 2000). The presence of integral feedback makes perfect adaptation a robust system feature that does not require a careful tuning of the system parameters, such as protein levels or rate constants. To demonstrate the robustness of this perfect adaptation, we measured the Hog1 response after changing the signaling fidelity of the MAPK cascade by controlling the expression of *PBS2*, which encodes the kinase of Hog1. To this end, we placed the genomic copy of *PBS2* under the inducible control of a Tet promoter. At saturating doxycycline levels, we observed Hog1-nuclear-enrichment dynamics comparable with wildtype cells (data not shown). By contrast, at low-level induction of the Tet promoter, the amplitude of the Hog1 response was significantly less than in wildtype, and we did not observe saturation in the peak amplitude as a function of salt (Figure 3C). Despite these gross differences, however, Hog1 nuclear enrichment still perfectly adapted. We conclude that integral feedback is a structural feature of the network; thus, perfect adaptation is a robust property of the system and not a consequence of precisely tuned parameters.

Strategy for Finding the Integrator

Our data begin to restrict the possibilities of where in the network the integrator can be. The potential locations we consider are four subsystems denoted *H*, *I*, *D*, and *G* (Figure 4). The *H* subsystem represents all relevant reactions that link an osmotic disturbance at the membrane with *H*og1 nuclear enrichment; for example, the MAPK cascade and nuclear-import reactions are in this subsystem. In the *D* subsystem are Hog1-*d*ependent mechanisms that promote glycerol accumulation, such as the transcriptional activation of genes that encode glycerol-producing enzymes and potential protein-protein interactions initiated by Hog1 in the cytoplasm or nucleus that lead to glycerol accumulation. In subsystem *I* are the Hog1-*i*ndependent mechanisms that contribute to osmolyte production, such as export-channel closure and gene-expression mediated by stress factors other than Hog1. Finally, subsystem *G* represents the metabolic reactions involved in *g*lycerol synthesis and any other reactions that contribute to glycerol accumulation. Positing that each subsystem either contains one or more integrators or contains none, we generated the 16 possible network configurations to guide our further analysis (Figure 4).

A critical aid in finding which of the subsystems contains the integrator(s) is the fact that with respect to the furthest-downstream integrator in a feedback loop, quantities upstream perfectly adapt, and those downstream do not (Supplemental Data). For instance, the observation that turgor pressure perfectly adapts—indeed, this is arguably the primary function of regulating osmotic stress—stipulates that at least one integrator must exist in *H*, *I*, *D*, or *G*, since turgor pressure is upstream of each of these systems within the feedback loop. This allows us to reject network configuration *(a)*, where none of the subsystems acts as an integrator. The observation of Hog1 perfect adaptation imposes an additional constraint: if the only integrator in the feedback loop were in subsystem *H*, then Hog1

nuclear enrichment would not perfectly adapt, because it is downstream of *H*. Thus, at least one of the subsystems *I*, *D*, and *G* must contain an integrator, permitting the rejection of configuration *(b)*.

The high-temporal resolution of our Hog1 measurements provides another severe constraint on possible network configurations. Our assay permits precise quantification of the area under the Hog1 curve (i.e., its integral). We find that in both wildtype cells and P_{Tet}-*PBS2* mutant cells, integrated-Hog1 scales linearly with the shock strength (Figure 3D) (note: the fact that their slopes differ does not affect the subsequent argument). If the system were composed only of reactions that could be modeled with linear dynamics, then such a result would be trivial; however, the fact that the peak Hog1 amplitude saturates as a function of salt (Figure 3A) is strong evidence of nonlinearity in the *H* subsystem and makes the data in Figure 3D quite informative. In particular, these data suggest that exactly one integrator exists between the input to subsystem *D* and the output of subsystem *G*, in addition, perhaps, to other serially arranged non-integrating subsystems with nearly linear input-output steady-state characteristics (Supplemental Data). We can reject the scenario in which both *D* and *G* are integrators since the double integral of Hog1 would be expected to scale linearly with shock strength, which is clearly not the case (Figure 3D, inset). Conversely, if neither *D* nor *G* is an integrator, then the fact that Hog1 perfectly adapts means that *I* must be an integrator. Not only do we experimentally refute this possibility in the next section, but we can also theoretically dismiss it because the nonlinearity in *H* would eliminate the linear scaling we observe between shock strength and integrated-Hog1. Thus, we conclude that either *D* is an integrator or *G* is an integrator, allowing us to reject configurations *(a)*, *(b)*, *(c)*, *(f)*, *(k)*, *(n)*, *(o)*, and *(p)*.

Perfect Adaptation Requires Hog1 Kinase Activity, Which Affects Glycerol Synthesis but not Leakage

To distinguish among the remaining putative network configurations, it was important to separate the roles of Hog1-dependent (*D* subsystem) and Hog1-independent (*I* subsystem) reactions. To this end, we mutated the endogenous Hog1 gene in our wildtype strain such that the kinase activity of the mutant (*hog1-as*) could be specifically, rapidly, and inducibly ablated by the ATP-analog 1-NM-PP1 ("PP1") (Westfall and Thorner, 2006). PP1 treatment has been shown to completely eliminate Hog1 kinase activity, unlike many of the previously studied constitutively "dead" isoforms, which were shown to retain both residual kinase activity (Westfall and Thorner, 2006) and the ability to perfectly adapt (Figure S4). In the presence of PP1, perfect adaptation is lost, as steady-state Hog1 accumulation does not return to its pre-stimulus level (Figure 5A). These results and those in Figure 5B were corrected for the effect PP1 has on cells not shocked with salt to isolate the salt-specific response (Figure S5, Experimental Procedures). Though the peak amplitude is less than in cells untreated with PP1 (Figure 5A, inset), this failure of PP1-treatred cells to adapt is not an artifact of the documented defect in nuclear transport of *hog1-as* (Westfall and Thorner, 2006) because nuclear enrichment dropped precipitously upon removal of the stimulus (Figure S6). Furthermore, the effect is specific to Hog1-kinase activity, since cells expressing wildtype Hog1 perfectly adapted even in the presence of PP1, though they, too, had diminished peak amplitude (Figure S7). Importantly, PP1-treatment eliminates the post-shock volume recovery (Figure 5B), suggesting that kinase-dead Hog1 persists in the nucleus because turgor pressure is not restored. We conclude that Hog1 kinase activity is necessary for the proper functioning of the integral-feedback controller in the osmoadaptation network.

Since PP1-treatment effectively severs the feedback loop between nuclear Hog1 and the Hog1-dependent mechanisms (i.e., it disconnects the *D* subsystem from its input), the loss of perfect adaptation further constrains the possible locations for the integrator(s). First, the

Hog1-independent subsystem (the *I* subsystem) cannot contain the last integrator in the feedback loop. If it did, then the turgor pressure would perfectly adapt in the presence of PP1, and Hog1 likely would as well, yet we observe neither (Figure 5A, B); thus, we reject scenarios *(c)*, *(f)*, *(i)*, and *(l)* from Figure 4. We can similarly reject scenarios where both *I* and *G* (the glycerol-accumulation subsystem) act as integrators (i.e., scenarios *(j)*, *(m)*, *(o)*, and *(p)*, Figure 4), since these scenarios would also ensure perfect adaptation in the system in the presence of PP1, which was not observed.

We expected that the failure of Hog1 nuclear enrichment to perfectly adapt in the absence of Hog1 kinase activity resulted from insufficient glycerol accumulation. Therefore, we compared internal glycerol accumulation in cells either treated or not treated with PP1. In cells not treated with PP1 ("−PP1"), intracellular glycerol rose rapidly after hyperosmotic shock but remained constant in unshocked cells (Figure 5C). In PP1-treated cells ("+PP1"), hyperosmotic shock caused a slight increase in internal glycerol, but the level achieved was significantly less than in −PP1 cells, consistent with loss of both turgor-pressure restoration and Hog1 perfect adaptation. There was a qualitative similarity between the traces of Hog1 nuclear enrichment and the rate of internal glycerol accumulation in −PP1 cells (compare Figure 3A and Figure 5D). Like the linear scaling of integrated-Hog1 with salt shock (Figure 3D), this correspondence is expected from network scenarios where exactly one integrator (in addition, perhaps, to some appropriate upstream and/or downstream linear subsystems) exists between Hog1 and glycerol. In the simplest case where the subsystem between Hog1 and glycerol contains only a single integrator and nothing else, the rate of glycerol accumulation would effectively be the derivative of the integral of Hog1 nuclear enrichment and should, therefore, be simply a scaled version of the Hog1 curve as observed. In +PP1 cells, where perfect adaptation is lost, this correspondence is also lost (compare Figure 5A, D) as the Hog1 and glycerol-accumulation-rate curves diverge at their post-stimulus steady-state levels (i.e., the rate of glycerol accumulation drops to zero, whereas Hog1 nuclear enrichment remains nonzero).

Insufficient glycerol accumulation in +PP1 cells prompted us to investigate the ways in which glycerol synthesis and leakage depend on Hog1 kinase activity. We measured cell-density-normalized levels of total glycerol and extracellular glycerol over time in the presence and absence of osmotic shock and PP1 (Figure 5E, F). In −PP1 cells, hyperosmotic shock leads rapidly to a transient decrease in glycerol leakage (Figure 5E) and a persistent increase in glycerol synthesis (Figure 5F) as compared to cells unstressed with salt. The results in +PP1 cells are partially influenced by a nonspecific effect of PP1. In the absence of salt shock, +PP1 cells increase glycerol synthesis and equivalently increase glycerol leakage, a behavior we found to be independent of Hog1 since it also occurred in cells with wildtype Hog1 (data not shown). Nonetheless, in +PP1 cells treated with salt, glycerol leakage is rapidly and transiently diminished, just as in −PP1 cells; yet the absence of Hog1 kinase activity prevents an increase in glycerol synthesis, unlike in −PP1 cells. Together, these data suggest that Hog1 kinase activity plays a critical role in rapidly regulating glycerol synthesis but not its leakage, consistent with a recent report (Westfall et al., 2008).

Neither Cell Volume Nor Hog1 Perfectly Adapts in Response to a Ramp Input

Four putative network configurations remain (Figure 4, *(d)*, *(e)*, *(g)*, and *(h)*), and we use an experiment motivated by control engineering to restrict the options even further. The key concept is that the number of integrators arranged in series in a system can be deduced by assaying for perfect adaptation in response to very specific input trajectories. In general, perfect adaptation to an input corresponding to the *n*th-integral of a step function implies that the system contains at least one feedback loop with at least *n+1* integrators arranged in series, where *n* is a positive integer. For the step input itself, where *n=0*, perfect adaptation demonstrates the existence of one or more integrators arranged in series. Perfect adaptation

in response to a linear-ramp input (*n=1*, since a ramp is simply the integral of a step) reveals the existence of two or more integrators in series, and so on.

We performed a flow-cell experiment in which the salt concentration ramps upward over time (Figure 6A), reaching a plateau after nearly 45 minutes. The slope of our ramp was chosen to reconcile two opposing factors: (1) that the ramp be steep enough to observe a signal in both volume and Hog1, and (2) that the ramp be shallow enough that both volume and Hog1 can reach steady state before the exterior salt concentration becomes so toxic that it occludes the response specific to the hyperosmotic shock system. In response to our ramp input and critically before the beginning of the plateau, we observed that neither volume nor Hog1 perfectly adapted (Figure 6B, C). Importantly, shortly after the plateau begins, both volume and Hog1 return to pre-stimulus levels, indicating that their failure to adapt in the presence of the ramp is specific to the stimulus itself and not because of the high final salt concentration of 0.75M.

The cell volume clearly reaches steady state within the ramp period and does not adapt, but it could be argued that Hog1 nuclear enrichment does not achieve steady state and could actually perfectly adapt were the ramp to persist for longer. Since even a pessimistic extrapolation of the pre-plateau Hog1 data would lead to perfect adaptation only after more than two hours, we argue that a second integrator permitting such adaptation is largely irrelevant because the extracellular salt concentration would be in excess of 2M at the time of adaptation, and the cells would almost certainly have perished.

In combination with our other findings, our ramp-input results confirm that there is exactly one integrator arranged in series in the system. This finding rejects many model configurations (Figure 4), but critically it invalidates *(g)* and *(h)*, which had not been otherwise refuted. We argue that the most likely network configuration is *(d)*, where subsystem *D* functions as an integrator and *G* does not. If *G* were to act as an integrator, then cell volume and turgor pressure would continue to recover as long as the input to the *G* subsystem is nonzero. But, when subsystem *D* is disabled in the presence of PP1, the only input to subsystem *G* is the output from subsystem *I*. Thus, the observed failure in volume recovery in PP1-treated cells (Figure 5B) would only occur if the output of subsystem *I* prematurely goes to zero (i.e., if it were a “differentiator”). This observation would require that all Hog1-independent mechanisms completely desensitize within approximately 20 minutes (i.e., the time needed for *hog1-as* nuclear enrichment to reach steady state; Figure 5B) despite persistence in their stimulus (i.e., the acute loss of turgor pressure). On the basis of this argument, we consider it extremely improbable that subsystem *G* acts an integrator. Therefore, we reject scenario *(e)*, leaving *(d)* as the last remaining configuration. We used a system of coupled differential equations to implement this concise model and found that it can indeed recapitulate the key features of our data (Figure S8, Supplemental Data). In sum, we conclude that the integrator responsible for perfect adaptation in response to a step input is a Hog1-dependent mechanism upstream of glycerol synthesis.

DISCUSSION

Using both biochemical techniques and engineering principles, we demonstrate that the low-noise (Figure 2), robust perfect adaptation of Hog1 nuclear enrichment and cell volume (Figure 3) results from a single integrating mechanism (Figure 4, 6) that requires Hog1 kinase activity (Figure 5A, B) and regulates glycerol synthesis (Figure 5E, F). Interestingly, despite a well-known role in mediating an osmostress-induced transcriptional response, Hog1 does not require gene expression to perfectly adapt (Figure S9, (Westfall et al., 2008)).

It is worth noting that our results are not inconsistent with multiple Hog1-kinase-dependent integrating reactions operating in parallel (our analysis here specifically rejects the possibility of multiple integrators in series). Redundant parallel integrating reactions would nonetheless yield one “effective” integrating mechanism, where each individual integrating reaction would strengthen the effective integrator and make the adaptation more rapid. Compared to a single integrating reaction, a parallel arrangement would also make the system more robust to mutation, since disabling one of the parallel integrating reactions would simply delay adaptation rather than prevent it altogether. Although future experiments will be required to determine exactly which reaction(s) is an integrator, the search may be facilitated by considering reactions downstream of Hog1 that are most likely to operate at saturation, since saturated reactions are one way to biologically implement integration (Supplemental Data) (Gomez-Uribe et al., 2007). We tested whether the series of reactions involving Hog1, Pfk26, and Pfk1,2 could be the integrator. Pfk26, which is activated in a Hog1-dependent manner after hyperosmotic stress (Dihazi et al., 2004), synthesizes factors that enhance the production of glycerol precursors by the highly abundant—and potentially saturating—Pfk1,2 complex. We knocked out *PFK2*, which has been shown to decrease the Pfk1,2 complex activity by nearly 95 percent (Arvanitidis and Heinisch, 1994) but saw no loss of perfect adaptation or appreciable delay in the adaptation kinetics (Figure S10), suggesting that this chain of reactions does not implement integral feedback. Other highly expressed substrates of Hog1 (Kim and Shah, 2007) should be investigated in the future for integrating properties.

A Dynamic Perspective on Hyperosmotic Shock Recovery

Our results yield the following dynamic portrayal of osmoregulation (Figure 7). In the absence of hyperosmotic shock, cells maintain a constant internal glycerol concentration. Glycerol is synthesized at a rate slightly higher than that required to keep pace with cell growth, and some glycerol is leaked (Figure 7, panel i). Within 20 seconds after a hyperosmotic shock, the cell volume drops to its minimum (Figure 2D), but Hog1 is not yet beginning to be enriched in the nucleus (Figure 2C), though some cytoplasmic Hog1 likely becomes activated and begins to upregulate glycerol synthesis (Figure 7, panel ii). After 20 seconds, the volume remains at its minimum but Hog1 becomes maximally enriched in the nucleus and glycerol synthesis continues to increase (Figure 7, panel iii). Beyond the first 5 minutes (Figure 7, panel iv), cell volume rises (Figure 2B and 3B), nuclear Hog1 accumulation begins to fall (Figure 2A and 3A), glycerol continues to be synthesized (Figure 5F), and some glycerol begins to leak to the exterior (Figure 5E). It is noteworthy that internal glycerol continues to increase beyond 15 minutes in −PP1 cells (Figure 6A) but not in +PP1 cells, indicating that +PP1 cells prematurely leak as much glycerol as they synthesize. If leakage prevention were stronger and/or endured for longer, then these cells could also accumulate enough glycerol to perfectly adapt; these data suggest that Hog1 kinase activity may play a role in the maintenance of glycerol retention beyond 15 minutes, though its effect may be indirect.

Beyond 25 minutes (Figure 7, panel v), the Hog1 nuclear enrichment returns to its pre-stimulus level (Figure 2A and 3A), the hallmark of perfect adaptation. Although the pre- and post-stimulus rates of glycerol accumulation are identical (Figure 6C, D), glycerol synthesis and leakage are significantly higher after the stimulus than before it (Figure 6E, F).

A Systematic Approach for Biological Systems Analysis

Our modeling efforts here and in *Mettetal et al.* underscore the power of applying engineering principles to any biological system that has well-defined and quantifiable inputs, internal variables, and outputs. In analyzing such systems, measurement of the frequency response (Mettetal et al., 2008) provides an estimate of the number of relevant

dynamic variables that a minimal model should have; additionally, these measurements may reveal the basic computation or function that the system performs. For systems potentially involving hundreds of reactions, each with unique kinetics, such analysis can appreciably reduce the complexity of a model without compromising, and potentially enhancing, the insight into systems-level behavior. Once the minimum number of dynamic variables has been estimated, the existing biochemical knowledge of the system can be leveraged to infer which biological quantities correspond to the relevant dynamic variables, and to create a basic network diagram such as the one in Figure 1B. Candidate molecules that may correspond to the relevant dynamic variables should include (1) factors known to be important in the system (e.g., glycerol and cell volume for the yeast osmotic-shock response), and (2) factors whose dynamics are expected to change on an appropriate timescale (e.g., fast protein-protein interactions versus slow gene-expression events). By measuring the dynamics of the internal variables in the system's network diagram, the model can be further constrained, and links can be drawn more confidently between model elements and biological mechanisms.

Perfect adaptation is one such dynamic feature that restricts potential models, where a basic result from control engineering provides important information about biological mechanism (Stelling et al., 2004). We expect similar analyses to be particularly useful in the study of other homeostatic systems that are ubiquitous in biology (e.g., blood calcium levels (El-Samad et al., 2002)), where perfect adaptation is presumably the paramount dynamic property of the network. Most of these systems likely achieve robust perfect adaptation through a negative feedback loop with one or more integrators; thus, an important future endeavor is to better understand how biological systems implement integration at the molecular level. Since the simple loss of integral feedback can fundamentally transform the function of a system—from one with transient output into one with persistent and potentially deleterious output—identifying and characterizing biological mechanisms providing integral feedback should be instrumental in the future study of homeostatic systems, the design of perfectly adapting biosynthetic circuits, and the development of therapeutics to combat disease.

EXPERIMENTAL PROCEDURES

Strain Background and Construction

Our haploid "wildtype" strain (DMY017) was derived from the DMY007 strain (Mettetal et al., 2008), the only difference being that the *SHO1* ORF was excised via standard PCR-based methods. Our PP1-sensitive strain (DMY034) was created by deleting the *HOG1* ORF from DMY017 (DMY030), generating a single-base mutation of *HOG1* on a plasmid using QuikChange (Stratagene), and then inserting the resulting *hog1-as* ORF (Westfall and Thorner, 2006) into DMY030 using PCR integration.

Fluorescence Microscopy and Image Analysis

Flow-chamber construction, cell preparation, image acquisition and image segmentation were all performed as described (Mettetal et al., 2008). For ramp experiments, a syringe pump (Harvard Apparatus) dispensed media containing concentrated NaCl into a graduated cylinder containing fresh media agitated by a magnetic stir bar. A peristaltic pump pulled liquid directly from the graduated cylinder into the flow cell. In both step and ramp experiments, each cell in an experiment is assigned an index. To quantify the Hog1 response of cell number i we compute the cell's raw nuclear enrichment $r_i(t)$, defined as the ratio of nuclear YFP intensity to whole-cell YFP intensity (a comparison of different quantification methods is in Supplemental Data, Figure S11). Specifically, the raw nuclear enrichment is

given by $r_i(t)=\frac{<y_{nuclear}>}{<y_{whole-cell}>}$, where the numerator is the average of the ten brightest nuclear pixels—unlike the average of the whole nucleus, this top-ten metric compensates for the diminishing ability to properly segment nuclear boundaries as Nrd1-RFP bleaches—and the denominator is the average intensity within the entirety of cell *i*.. Defining $r_i(t)$ as a ratio of YFP intensities provides some correction for photo-bleaching.

We define the Hog1 nuclear enrichment, $h_i(t)$, of cell number *i* by $h_i(t)=\frac{r_i(t)}{r_i(t_0)}-1$, where $r_i(t_0)$ is the raw nuclear enrichment of cell number *i* before osmostress. We estimate $r_i(t_0)$ by the average raw nuclear enrichment for the four preshock time points.

To quantify single-cell volume, we first compute the number of pixels $n_i(t)$ that constitute cell number *i* as a function of time. This number is proportional to the cell's area, so assuming that the cell is a sphere, $(n_i(t))^{1.5}$ is directly proportional to the volume. We define the relative volume increase, $v_i(t)$, of cell number *i* by $v_i(t)=\left(\frac{n_i(t)}{n_i(t_0)}\right)^{\frac{3}{2}}-1$. Here $n_i(t_0)$ is the pre-shock number of pixels of cell number *i*, which we estimate by taking the average of $n_i(t)$ over the four pre-shock time points.

To correct the Hog1 and volume data from our +PP1 and +CHX experiments, we subtract the mean trace (N≥3) in unstressed cells (i.e., an hour-long experiment with only 0M [NaCl]; Figure S5) from the mean trace in stressed cells (N≥3). We assume the error in stressed and unstressed experiments is independent, so we add the respective variances and then calculate the standard error of our corrected mean trace.

Glycerol Assays

Glycerol levels were measured using the Free Glycerol Reagent Kit (Sigma). For details about preparing cells and separately acquiring intracellular, extracellular, and total glycerol levels, see Supplemental Data.

Supplementary Material

Refer to Web version on PubMed Central for supplementary material.

Acknowledgments

We thank J. Falvo, R. Tsien, and E. O'Shea for the mRFP1.3 plasmid, as well as Suzanne Komili, George Verghese and Leonid Mirny for insightful comments and discussions. This work was supported by NSF Graduate Research Fellowships to D.M. and J.T.M., a MIT-Merck Graduate Fellowship to C.A.G-U., and NIH grants R01-GM068957 and 5 R90 DK071511-01.

References

Arvanitidis A, Heinisch JJ. Studies on the function of yeast phosphofructokinase subunits by in vitro mutagenesis. J Biol Chem. 1994; 269:8911–8918. [PubMed: 8132627]

Barkai N, Leibler S. Robustness in simple biochemical networks. Nature. 1997; 387:913–917. [PubMed: 9202124]

Cai L, Dalal CK, Elowitz MB. Frequency-modulated nuclear localization bursts coordinate gene regulation. Nature. 2008; 455:485–490. [PubMed: 18818649]

Dihazi H, Kessler R, Eschrich K. High osmolarity glycerol (HOG) pathway-induced phosphorylation and activation of 6-phosphofructo-2-kinase are essential for glycerol accumulation and yeast cell

proliferation under hyperosmotic stress. J Biol Chem. 2004; 279:23961–23968. [PubMed: 15037628]

El-Samad H, Goff J, Khammash M. Calcium homeostasis and parturient hypocalcemia: an integral feedback perspective. J Theor Biol. 2002; 214:17–29. [PubMed: 11786029]

Ferrigno P, Posas F, Koepp D, Saito H, Silver P. Regulated nucleo/cytoplasmic exchange of HOG1 MAPK requires the importin beta homologs NMD5 and XPO1. EMBO J. 1998; 17:5606–5614. [PubMed: 9755161]

Gennemark P, Nordlander B, Hohmann S, Wedelin D. A simple mathematical model of adaptation to high osmolarity in yeast. In Silico Biol (Gedrukt). 2006; 6:193–214. [PubMed: 16922683]

Gomez-Uribe C, Verghese G, Mirny L. Operating regimes of signaling cycles: statics, dynamics, and noise filtering. PLoS Comput Biol. 2007; 3:e246. [PubMed: 18159939]

Hersen P, McClean MN, Mahadevan L, Ramanathan S. Signal processing by the HOG MAP kinase pathway. Proc Natl Acad Sci U S A. 2008; 105:7165–7170. [PubMed: 18480263]

Hohmann S. Osmotic stress signaling and osmoadaptation in yeasts. Microbiol Mol Biol Rev. 2002; 66:300–372. [PubMed: 12040128]

Hohmann S, Krantz M, Nordlander B. Yeast osmoregulation. Meth Enzymol. 2007; 428:29–45. [PubMed: 17875410]

Ingalls, B.; Yi, T.; Iglesias, P. Using Control Theory to Study Biology. In: Szallasi, Z.; Stelling, J.; V, P., editors. System Modeling in Cellular Biology. Cambridge, MA: MIT Press; 2006. p. 243-267.

Kim S, Shah K. Dissecting yeast Hog1 MAP kinase pathway using a chemical genetic approach. FEBS Lett. 2007; 581:1209–1216. [PubMed: 17346711]

Klipp E, Nordlander B, Krüger R, Gennemark P, Hohmann S. Integrative model of the response of yeast to osmotic shock. Nat Biotechnol. 2005; 23:975–982. [PubMed: 16025103]

Luyten K, Albertyn J, Skibbe W, Prior B, Ramos J, Thevelein J, Hohmann S. Fps1, a yeast member of the MIP family of channel proteins, is a facilitator for glycerol uptake and efflux and is inactive under osmotic stress. EMBO J. 1995; 14:1360–1371. [PubMed: 7729414]

McClean M, Mody A, Broach J, Ramanathan S. Cross-talk and decision making in MAP kinase pathways. Nat Genet. 2007; 39:409–414. [PubMed: 17259986]

Mettetal J, Muzzey D, Gómez-Uribe C, van Oudenaarden A. The frequency dependence of osmo-adaptation in Saccharomyces cerevisiae. Science. 2008; 319:482–484. [PubMed: 18218902]

Newman JR, Ghaemmaghami S, Ihmels J, Breslow DK, Noble M, DeRisi JL, Weissman JS. Single-cell proteomic analysis of S. cerevisiae reveals the architecture of biological noise. Nature. 2006; 441:840–846. [PubMed: 16699522]

O'Rourke S, Herskowitz I. Unique and redundant roles for HOG MAPK pathway components as revealed by whole-genome expression analysis. Mol Biol Cell. 2004; 15:532–542. [PubMed: 14595107]

Proft M, Struhl K. MAP kinase-mediated stress relief that precedes and regulates the timing of transcriptional induction. Cell. 2004; 118:351–361. [PubMed: 15294160]

Reed R, Chudek J, Foster R, Gadd G. Osmotic significance of glycerol accumulation in exponentially growing yeasts. Appl Environ Microbiol. 1987; 53:2119–2123. [PubMed: 3314706]

Reiser V, Raitt D, Saito H. Yeast osmosensor Sln1 and plant cytokinin receptor Cre1 respond to changes in turgor pressure. J Cell Biol. 2003; 161:1035–1040. [PubMed: 12821642]

Schoeberl B, Eichler-Jonsson C, Gilles E, Müller G. Computational modeling of the dynamics of the MAP kinase cascade activated by surface and internalized EGF receptors. Nat Biotechnol. 2002; 20:370–375. [PubMed: 11923843]

Schwartz M, Madhani H. Principles of MAP kinase signaling specificity in Saccharomyces cerevisiae. Annu Rev Genet. 2004; 38:725–748. [PubMed: 15568991]

Slaninová I, Sesták S, Svoboda A, Farkas V. Cell wall and cytoskeleton reorganization as the response to hyperosmotic shock in Saccharomyces cerevisiae. Arch Microbiol. 2000; 173:245–252. [PubMed: 10816042]

Sontag E. Adaptation and regulation with signal detection implies internal model. Syst Control Lett. 2003; 50:119–126.

Stelling J, Sauer U, Szallasi Z, Doyle F, Doyle J. Robustness of cellular functions. Cell. 2004; 118:675–685. [PubMed: 15369668]

Tamás M, Rep M, Thevelein J, Hohmann S. Stimulation of the yeast high osmolarity glycerol (HOG) pathway: evidence for a signal generated by a change in turgor rather than by water stress. FEBS Lett. 2000; 472:159–165. [PubMed: 10781825]

Westfall P, Thorner J. Analysis of mitogen-activated protein kinase signaling specificity in response to hyperosmotic stress: use of an analog-sensitive HOG1 allele. Eukaryotic Cell. 2006; 5:1215–1228. [PubMed: 16896207]

Westfall PJ, Patterson JC, Chen RE, Thorner J. Stress resistance and signal fidelity independent of nuclear MAPK function. Proc Natl Acad Sci U S A. 2008; 105:12212–12217. [PubMed: 18719124]

Yi T, Huang Y, Simon M, Doyle J. Robust perfect adaptation in bacterial chemotaxis through integral feedback control. Proc Natl Acad Sci USA. 2000; 97:4649–4653. [PubMed: 10781070]

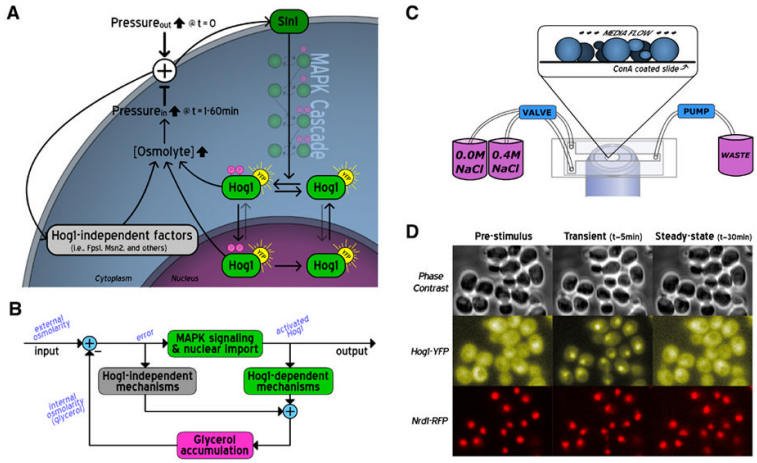

Figure 1. Hog1 translocates to the nucleus in response to hyperosmotic shock

(A) An upward spike in external osmotic pressure at t=0 is sensed by Sln1, which propagates a signal via a MAPK cascade that culminates in the dual phosphorylation and nuclear import of Hog1. In the nucleus, Hog1 activates gene expression; active Hog1 also plays various roles in the cytoplasm to facilitate osmoadaptation. Together with Hog1-independent stress responses, these mechanisms increase internal glycerol, thereby restoring turgor pressure across the membrane. Our "wildtype" strain has YFP fused to Hog1, and the Sln1 branch is the primary osmosensor, since *SHO1* is deleted.

(B) Network diagram inferred from (A) showing the system input and measurable outputs.

(C) Schematic of our simple flow chamber. The pump draws media through the flow-cell, with the osmolarity controlled by a valve. Cells adhere to the coverslip coated with 1 mg/ml conA in water.

(D) Phase-contrast (top row), Hog1-YFP (middle row), and Nrd1-RFP (bottom row) images are captured at each time point. In the absence of hyperosmotic shock, Hog1-YFP is distributed throughout the cell (left column). Only transiently does Hog1 accumulate appreciably in the nucleus after a shock (middle column), restoring the pre-stress distribution at steady state (right column).

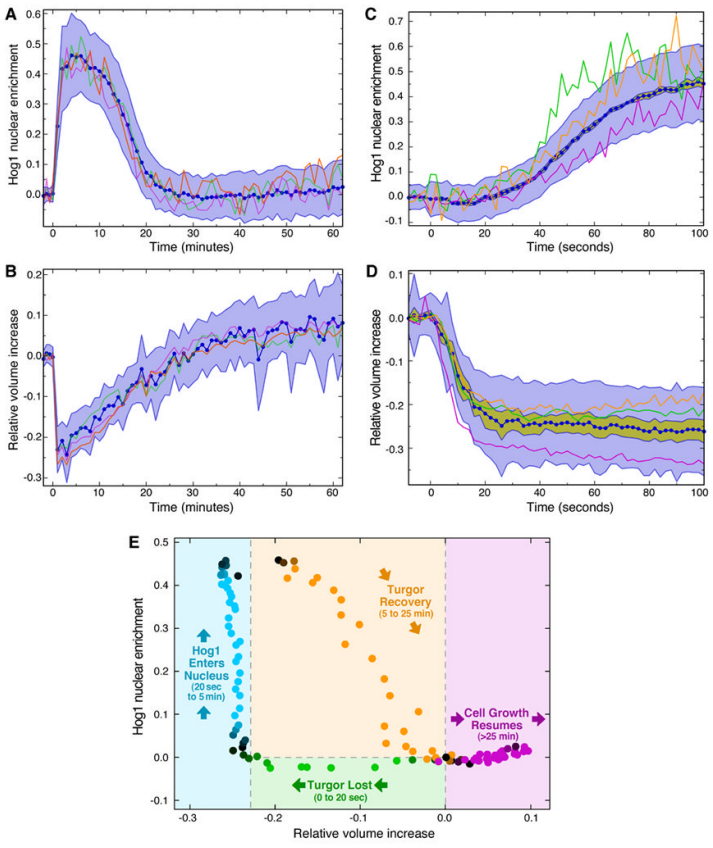

Figure 2. MAPK signaling introduces very little cell-to-cell variability in Hog1 nuclear enrichment

(A) In response to a step shock of 0.4M NaCl, dynamics in single-cell Hog1 nuclear enrichment (shown for three cells in green, orange, and purple; defined in Experimental Procedures) strongly resemble the population average (dark-blue dotted line) obtained from a single experiment (>100 cells). The shaded region is +/− STD around the population average and represents the cell-to-cell variability of a single experiment.

(B) Cell volume traces are low in noise (salt stimulus, single cells, mean, and shaded area are as in (A)). After an abrupt decrease in cell volume after t = 0, volume recovers and exceeds the pre-stimulus value, indicative of cell growth within the flow cell once turgor pressure is restored.

(C) and (D) Two-second sampling of single-cell Hog1 nuclear enrichment (C) and cellular volume (D) (salt stimulus, single cells, mean, and blue shaded area are as in (A)). Yellow shaded region depicts +/− SEM for >3 independent flow cells.

(E) For each time point in panels (A) through (D), the cell volume and Hog1 nuclear enrichment values are positioned on this scatter plot of Hog1 versus volume, illustrating four distinct regions. Spots are false-colored for clarity, becoming black near the boundaries between regions.

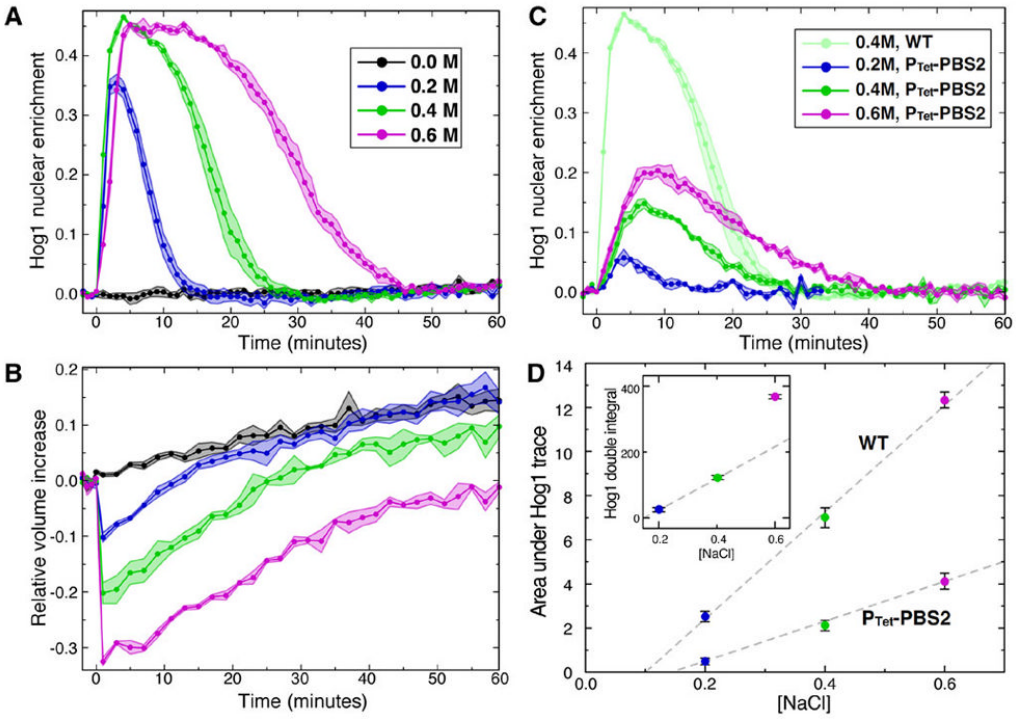

Figure 3. Hog1 nuclear enrichment exhibits robust perfect adaptation

(A) In response to hyperosmotic shocks with indicated concentrations of NaCl, the steady-state Hog1 nuclear enrichment returns exactly to the same level as in unshocked cells. All cells were grown and loaded into the flow cell using media with 0.0 M NaCl. Dotted lines show the average response, obtained by averaging population averages from independent experiments (N=3 or 4); error boundaries depict +/− SEM.

(B) Cell volume traces corresponding to the experiments in (A), except that all post-shock data points are the average of measurements at three consecutive time points.

(C) Hog1 nuclear enrichment perfectly adapts even in cells with compromised MAPK signaling. The TetO7 promoter was integrated upstream of the endogenous *PBS2* gene. In the experiments shown, [doxycycline] = 0.06 μg/ml.

(D) The area under the Hog1 curves in (A) and (C) scales linearly with [NaCl] consistent with a single integrator between Hog1 activation and glycerol accumulation (Supplemental Data); dotted gray lines are guides for the eye. Data points indicate mean +/− STD of the area calculated from at least three independent Hog1-nuclear-enrichment traces. The inset shows the double integral of Hog1 curves in (A), calculated up to the point where the data curves adapt.

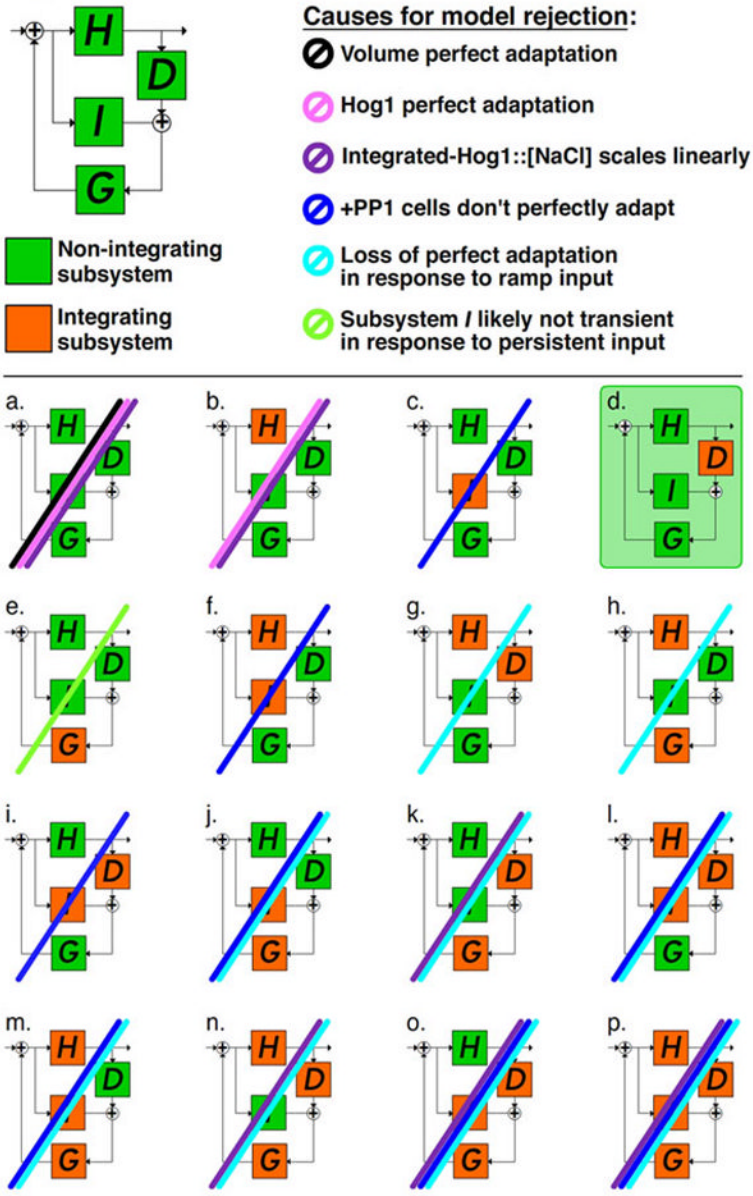

Figure 4. Perfect adaptation and other data reject many potential network schematics

We permute the model from Figure 1B (shown in reduced form at top-left) such that each of the subsystems *H*, *D*, *I*, and *G*, is an integrator (shaded orange) or not (shaded green), yielding the sixteen possibilities *(a)* through *(m)*. For the reasons listed at top-right, which consider data from Figures 2, 3, 5, and 6, certain network schematics can be rejected. Only network *(d)* satisfies all the constraints.

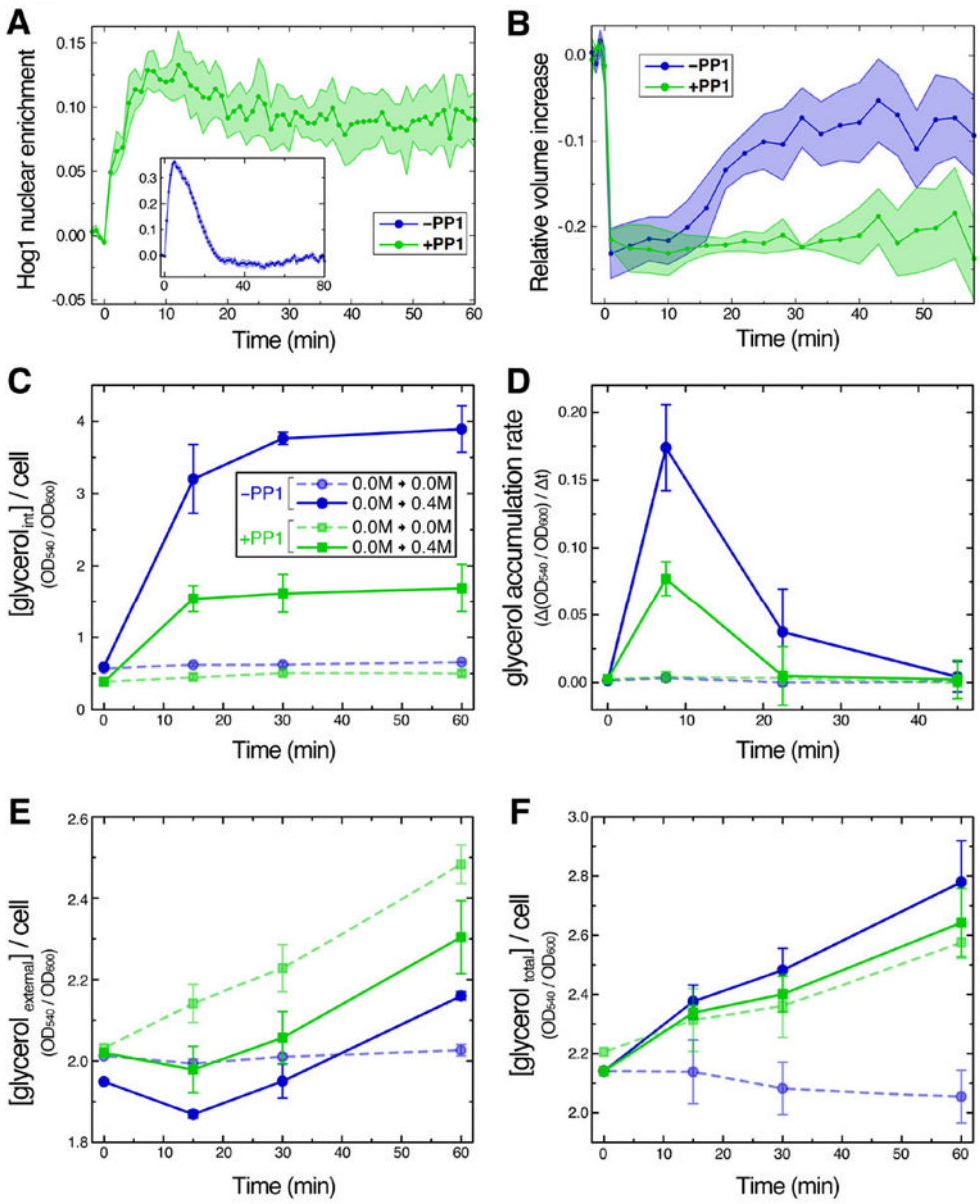

Figure 5. Hog1 kinase activity is required for perfect adaptation of Hog1 nuclear enrichment and glycerol accumulation via a role in upregulating glycerol synthesis

(A) Nuclear enrichment of (*hog1-as*)-YFP in cells treated with 24 μM PP1 prior to hyperosmotic shock with 0.4 M NaCl. This trace is corrected to highlight the salt-specific response (Figure S3). In the inset, the same strain is stressed in the same manner, except PP1 is omitted. In both the main curve and the inset, the mean (N=3) +/− SEM is plotted.

(B) Mean volume traces (N=3) +/− SEM from the corresponding experiments in (A), again corrected to highlight the salt-specific response (Figure S3).

(C) Dynamics in the concentration of intracellular glycerol (OD_{540} measurement from glycerol kit; see Experimental Procedures), corrected for cell-growth (OD_{600} measurement) by taking the ratio, were measured in *hog1-as* cells in the presence and absence of 24 μM PP1 (administered 30 minutes before experiment) and hyperosmotic shock with 0.4 M NaCl (administered at t = 0). Data points represent the mean (N=3) +/− STD.

(D) The glycerol accumulation rate was computed as the slope of the traces in (A), and the time of each plotted point corresponds to the midpoint of the two time points used in the slope computation (e.g., the slope between the 0-minute and 15-minute time points is plotted at 7.5 minutes). Error bars represent the combined standard deviation from data points in (A), assuming measurements were independent at different time points.
(E) and (F): Dynamics in the extracellular (E) and total (F) glycerol concentration (see Experimental Procedures) in experiments outlined in (C) and described in the main text. Data points and error bars are as described in (C).

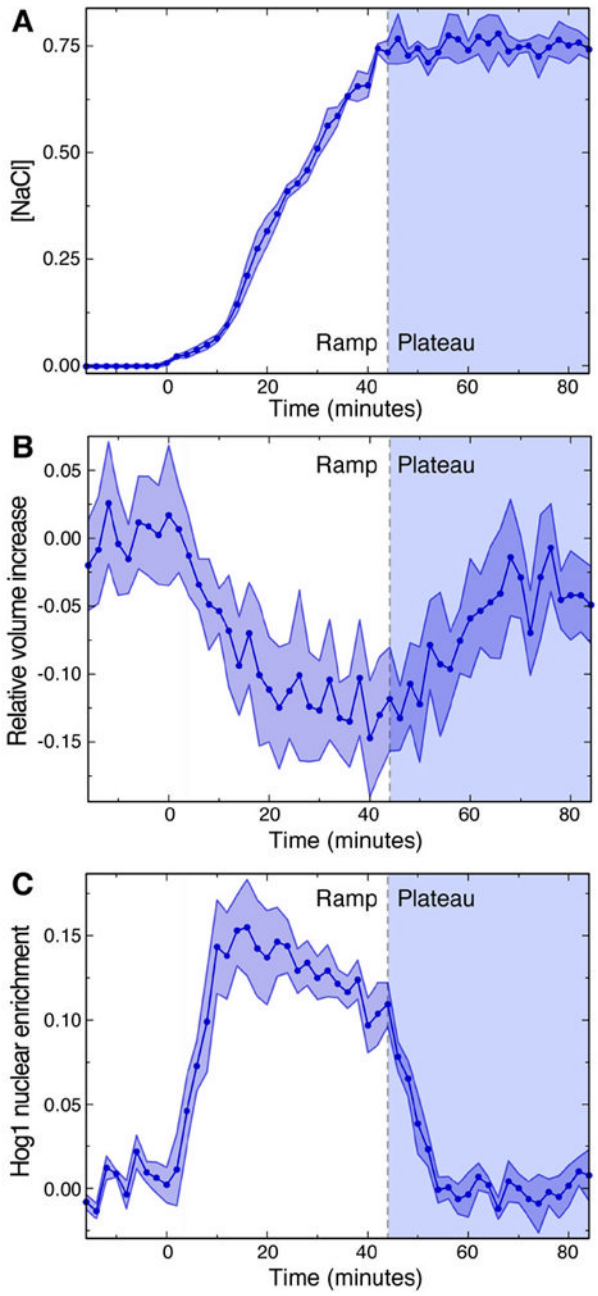

Figure 6. Neither cell volume nor Hog1 nuclear enrichment perfectly adapts in response to a ramp input

(A) The calculated concentration of NaCl in the flow chamber as a function of time (see Experimental Procedures). We measured the fluorescence intensity of rhodamine diluted in water and converted to [NaCl] based on the respective dilutions. The mean (N=3) +/− SEM is shown.

(B) and (C) Temporal changes in relative volume increase (B) and Hog1 nuclear enrichment (C) in response to ramp input shown in (A) (mean and error are same as in (A)). During the ramp period, volume and Hog1 fail to perfectly adapt, but they later adapt during the plateau period.

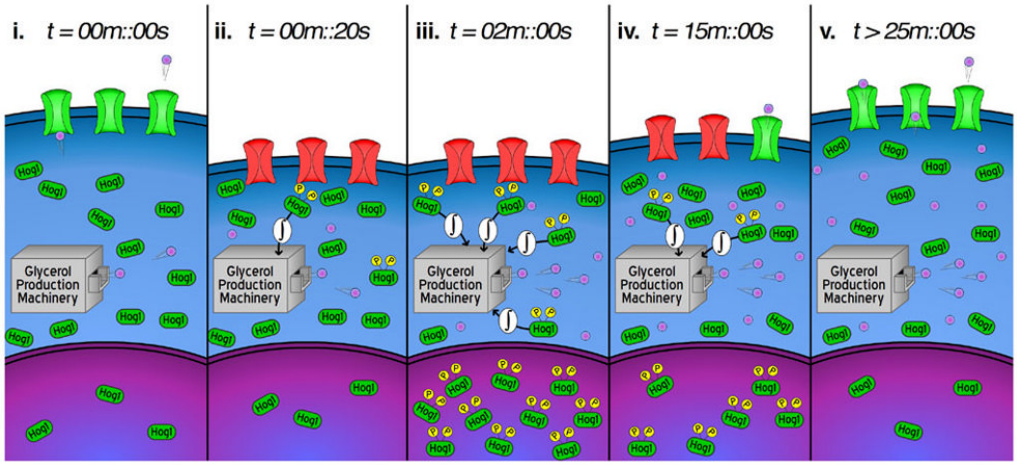

Figure 7. A simple model based on our data captures key data features

Cartoon representation of key features of yeast hyperosmotic shock response, explained in detail in the Discussion. Hyperosmotic shock is applied at t = 0. Green membrane channels are open, allowing the transport of glycerol, shown as purple circles. Upon closure, the channel is depicted in red.